Supporting Information

Dual-Function Electrolyte Design Enabling Sulfur Redox-Mediated Charging and Anode Stabilization in Zn-Air Batteries

Fei Huang,[a] Yuhao Zhang,[a] Fei Zhang,[a] Xinjunqi Yuan,[a] Wei Chen,[b] Lei Zhang,*[c] Changfei Sun,[d] CongChen,*[d] Haibo Hu,[b] Nadeem Hussain*[b]

Dr. F. Huang, Y. H. Zhang, F. Zhang, X. J. Q. Yuan

[a] School of Chemistry and Chemical Engineering, HuangShan University, Huangshan 245041, China.

W. Chen, Dr. Haibo Hu, and Dr. N. Hussain

[b] School of Materials Science and Engineering, Anhui University, Hefei 230601, China.
Email: nadeem8742@ahu.edu.cn

Dr. L. Zhang

[c] School of Energy, Materials and Chemical Engineering, Hefei University, Hefei, 230601, China
Email: zhanglei@hfuu.edu.cn

C. F. Sun, and Dr. C. Chen

[d] School of Chemistry and Materials Science, Qinghai Minzu University, Xining 810007, China. Email: 2016016@qhmu.edu.cn

Experimental Section

Materials

Iron (III) nitrate nonahydrate ($Fe(NO_3)_2·9H_2O$, AR), nickel (II) nitrate hexahydrate ($Ni(NO_3)_2·6H_2O$, AR), glucose ($C_6H_{12}O_6$, AR), potassium hydroxide (KOH, AR), dihydrodiamine ($C_2H_4N_4$, AR), urea (CH_4N_2O, AR), thiourea (CH_4N_2S, AR), allantoin ($C_4H_6N_4O_3$, AR), dipotassium sulphide (K_2S, AR), isopropanol (C_3H_8O, AR) were all purchased from Aladdin Scientific Corporation. Nafion solution was purchased from Shanghai Macklin Biochemical Technology Co., Ltd. All reagents were analytical grade, and no further purification was required.

Synthesis of Ni_3Fe@CNTs

Ni_3Fe alloy nanoparticles anchored on carbon nanotubes (Ni_3Fe@CNTs) were synthesized via a one-step in-situ pyrolysis method. Typically, 5 g of dihydrodiamine, 0.25 g of glucose, 0.25 g of $Ni(NO_3)_2·6H_2O$, and 0.1 g of $Fe(NO_3)_2·9H_2O$ were dissolved in 100 mL of deionized water and stirred vigorously for 8 h. The homogeneous solution was then dried in an oven at 80 °C for 12 h to obtain a powdered precursor.

During pyrolysis, dihydrodiamine and glucose serve as the carbon and nitrogen sources for CNT growth, while nickel and iron nanoparticles act as the catalyst for the in-situ formation of carbon nanotubes. To obtain the final product, the precursor powder was placed in a tube furnace and heated under a continuous flow of high-purity nitrogen (N_2). Prior to heating, the furnace tube was purged with N_2 at a flow rate of 200 sccm for 30 min to completely remove any residual oxygen. Subsequently, the temperature was ramped to 900 °C at a heating rate of 5 °C min^{-1} and maintained at 900 °C for 2 h under a constant N_2 flow of 100 sccm. After natural cooling to room temperature under the same N_2

atmosphere, the resulting black powder was collected and designated as Ni_3Fe@CNTs. The inert atmosphere throughout the process prevents oxidation of carbon nanotubes and the alloy nanoparticles.

Structure and composition characterization

The crystal structure of the sample was analyzed using an 18 kW advanced X-ray diffractometer (XRD Bruker D8-ADVANCE) with Cu Kα radiation (λ=1.54056Å). Morphological and elemental characterization was achieved through field emission scanning electron microscopy (FE-SEM) and transmission electron microscopy (TEM), which provided high-resolution imaging of microstructural features and energy-dispersive X-ray spectroscopy (EDS) mapping of elemental distributions. The valence states and bonding modes of the materials were analyzed using X-ray photoelectron spectroscopy (XPS). Optical properties were evaluated via UV-visible spectroscopy (Shimadzu UV-M4).

Electrochemical measurement

All linear sweep voltammetry (LSV) tests were conducted using an electrochemical workstation (660E, Chenhua, Shanghai) following the standard three-electrode setup. Platinum wire was employed as the counter electrode, the reference electrode was Ag/AgCl, and the disk electrode was glassy carbon (GC). The electrolyte was a 0.1 M KOH / 0.1 M KOH+0.05 M Thiourea solution. The potential measurements were referenced to RHE, where $E_{RHE} = E_{Ag/AgCl} + 0.059\ pH + E^{\theta}_{Ag/AgCl}$. The rotating disk electrode (RDE) served as the working electrode throughout the experiment. A 10 mg catalyst was dispersed in a mixed solvent of 250 μl isopropanol, 700 μl deionized water, and 50 μl Nafion solution (5 wt%). The solution was then ultrasonicated for 60 minutes to ensure a uniform mixture

of the catalyst ink. Subsequently, 8 μl of the catalyst ink droplets were deposited onto the glass carbon (GC) rotating disk electrode (5 mm in diameter) and dried completely at room temperature before testing. In alkaline media, the RDE test was conducted at room temperature in O_2-saturated 0.1 M KOH solution. Under the same conditions, oxygen evolution reaction (OER) measurements were performed with a rotation rate of 1600 rpm.

Fabrication of liquid Zn-air batteries

The liquid zinc-air batteries were fabricated using the following procedure. The catalyst ink was first prepared according to the previously described standard method. This ink was then uniformly deposited onto a hydrophobic carbon paper substrate to form the air cathode, with the catalyst loading carefully maintained at 1.0 $mg \cdot cm^{-2}$. A polished zinc foil was employed as the anode. The electrolyte used was 6 M KOH aqueous solution, either with or without the addition of 0.05 M thiourea, depending on the experimental design. Finally, the battery was assembled in a custom-designed electrochemical cell by integrating the prepared air cathode, zinc anode, and electrolyte, ensuring proper alignment and sealing to maintain consistency across all electrochemical tests.

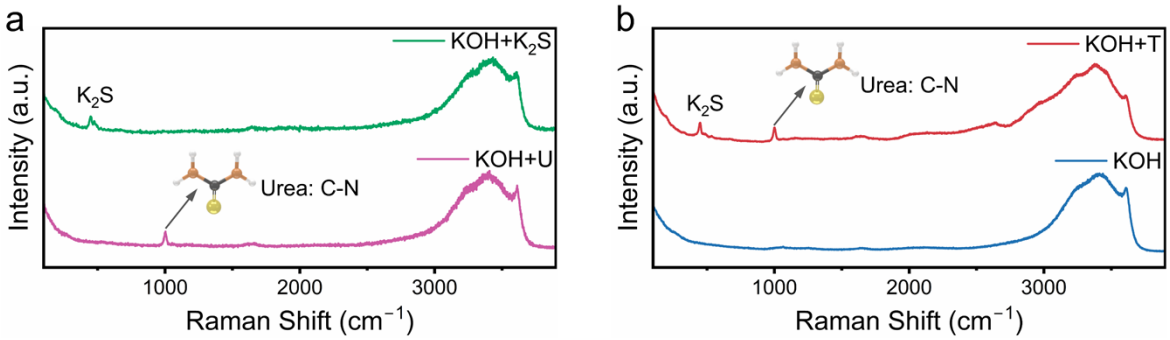

Figure S1. a, b) Raman spectra of different additives in KOH electrolyte.

Figure S2. Scheme illustration for the synthetic procedure of Ni_3Fe@CNTs.

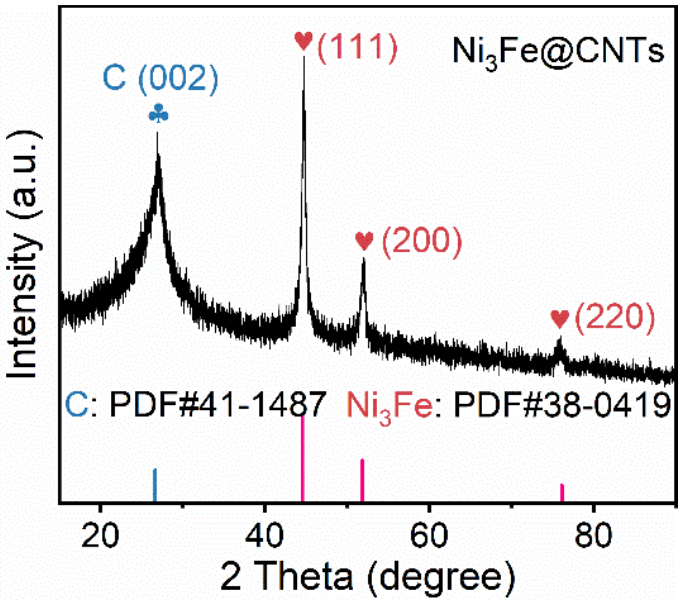

Figure S3. XRD pattern of Ni_3Fe@CNTs.

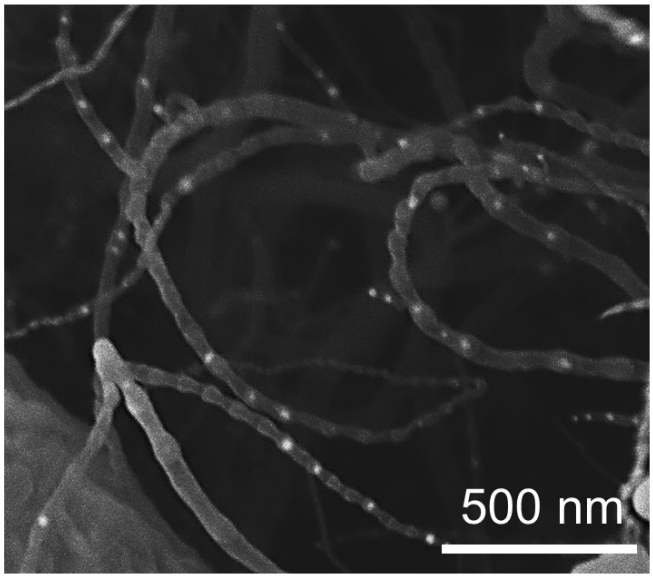

Figure S4. SEM images of Ni_3Fe@CNTs.

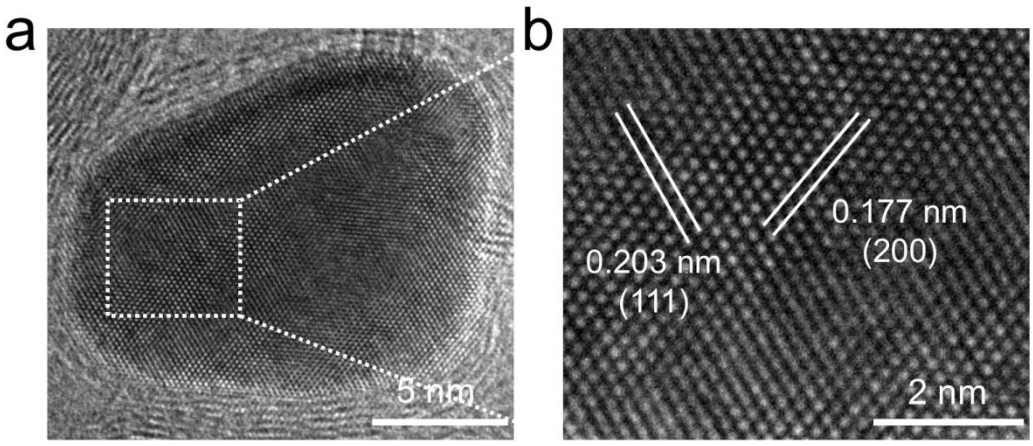

Figure S5. a) TEM and b) the corresponding localized HR-TEM images of Ni_3Fe@CNTs.

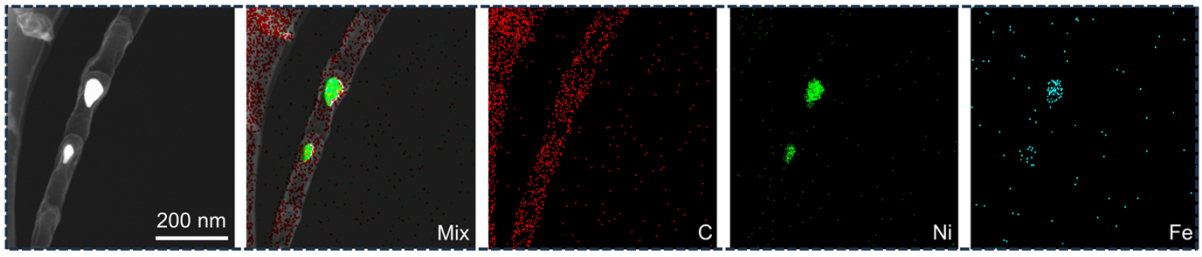

Figure S6. TEM image and the corresponding EDS mapping images of Ni_3Fe@CNTs.

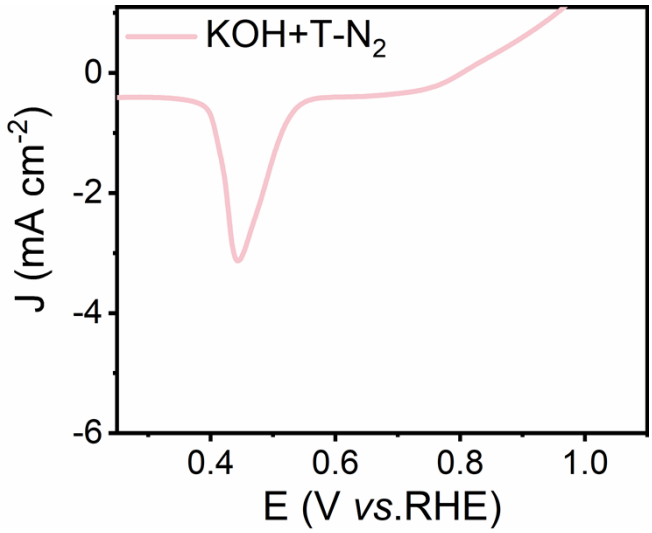

Figure S7. LSV curves in 0.1 M KOH + 0.05 M thiourea solution under N_2 atmosphere.

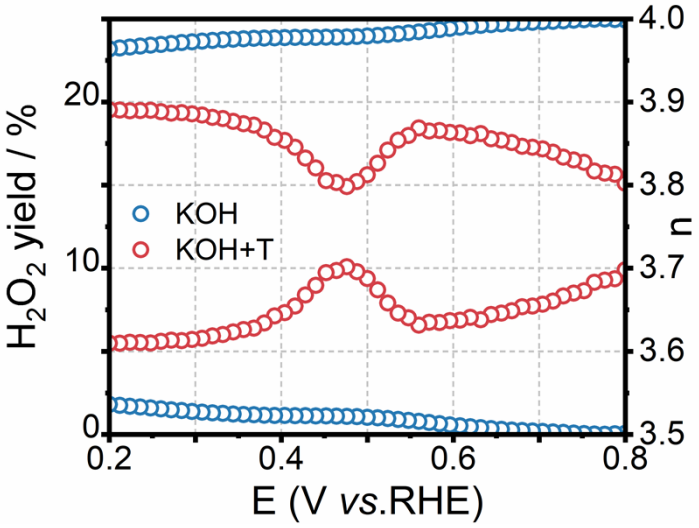

Figure S8. Peroxide yield and electron transfer number for the samples based on RRDE voltammograms at a rotating speed of 1600 rpm in O_2-saturated 0.1M KOH and 0.1M KOH+0.05M Thiourea (KOH+T).

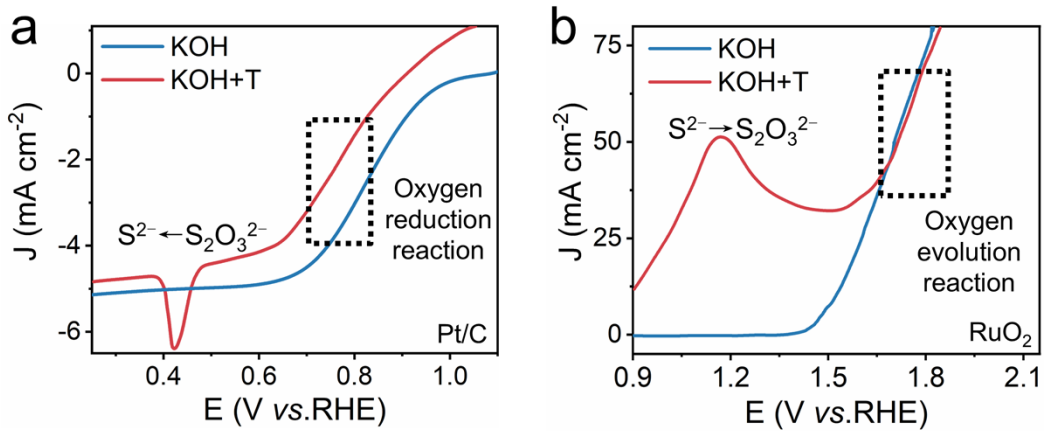

Figure S9. LSV curves of a) Pt/C and b) RuO_2 in KOH and KOH+T (Blue: 0.1 M KOH, Red: 0.1 M KOH+0.05 M Thiourea).

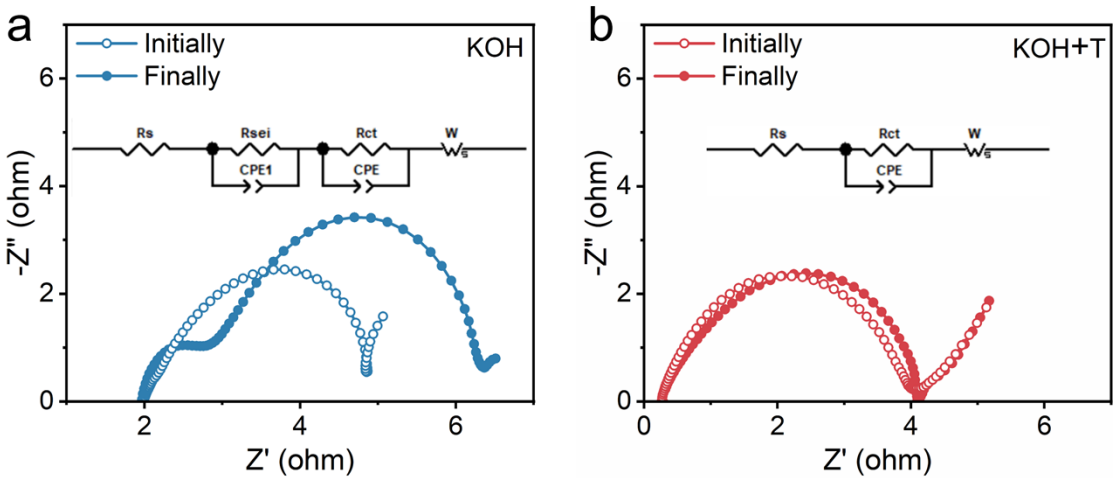

Figure S10. The electrochemical impedance spectra of zinc-air batteries in a) KOH and b) KOH+T solution (from initial state to final state).

For KOH-ZABs:

Rs: Ohmic resistance of the electrolyte and cell components.

Rsei|CPE1: Resistance and constant phase element associated with the solid electrolyte interphase (SEI) layer formed on the zinc anode.

Rct|CPE: Charge transfer resistance and double-layer capacitance at the electrode/electrolyte interface.

W: Warburg impedance representing diffusion of species in the electrolyte.

For KOH+T-ZABs:

Rs: Ohmic resistance.

Rct|CPE: Charge transfer resistance and double-layer capacitance.

W: Warburg impedance.

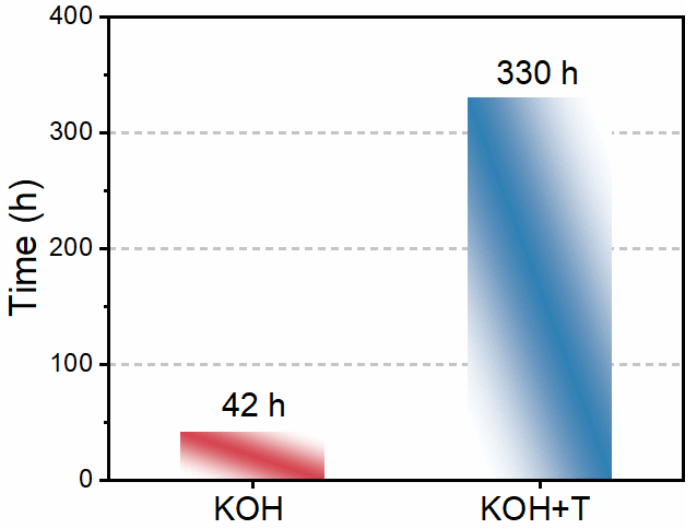

Figure S11. Comparison of cycle time of ZABs with KOH and KOH+T electrolytes.

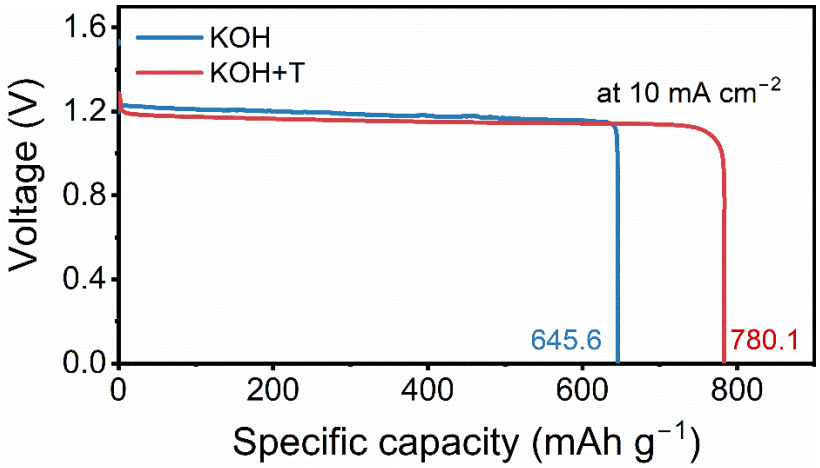

Figure S12. Galvanostatic discharge curves of ZABs with KOH and KOH+T electrolytes at 10 mA cm^{-2}. The specific capacity is calculated based on the mass of zinc consumed.

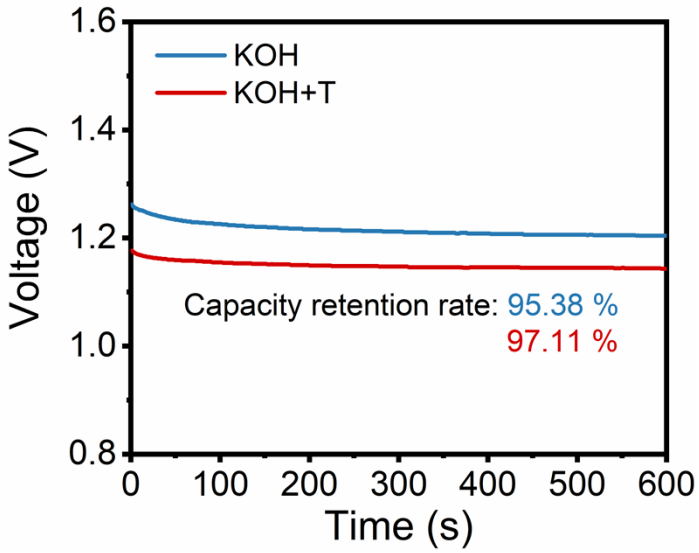

Figure S13. Self-discharge behavior of ZABs with KOH and KOH+T electrolytes.

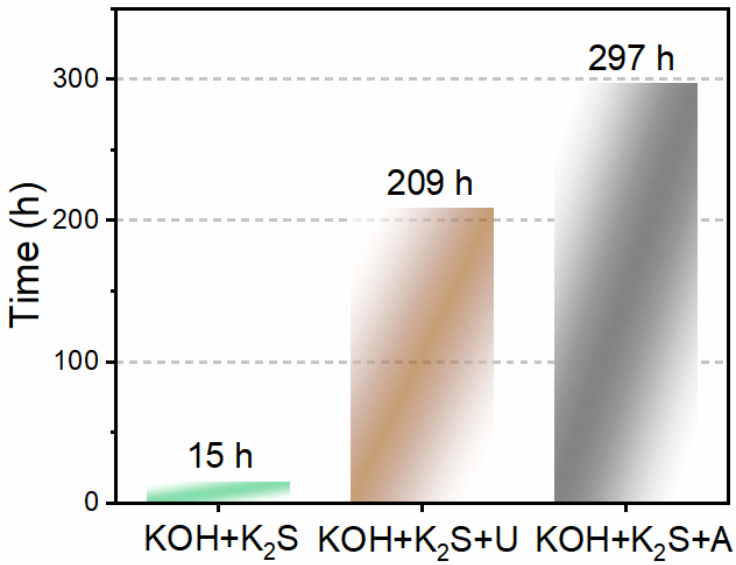

Figure S14. Comparison of cycle time of ZABs with KOH+K_2S, KOH+K_2S+U and KOH+K_2S+A electrolytes.

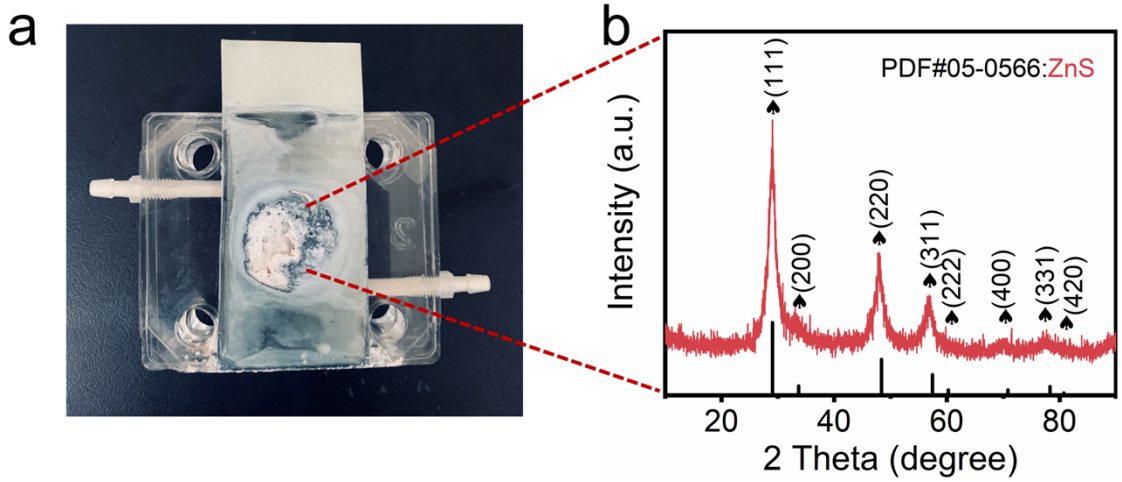

Figure S15. a) Optical image of zinc foils after battery failure and b) the corresponding XRD pattern (white precipitate).

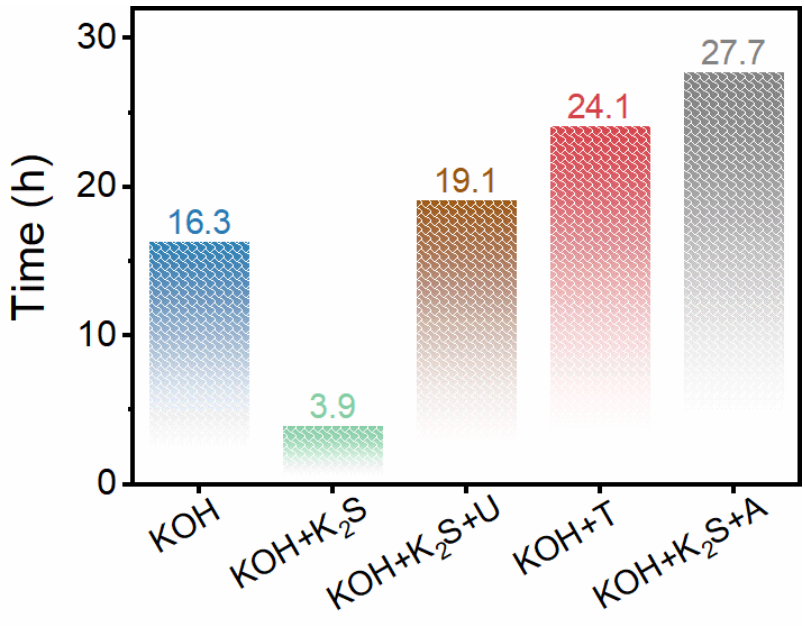

Figure S16. Comparison of cycle time of Zn⊠Zn symmetric cells with different electrolytes.

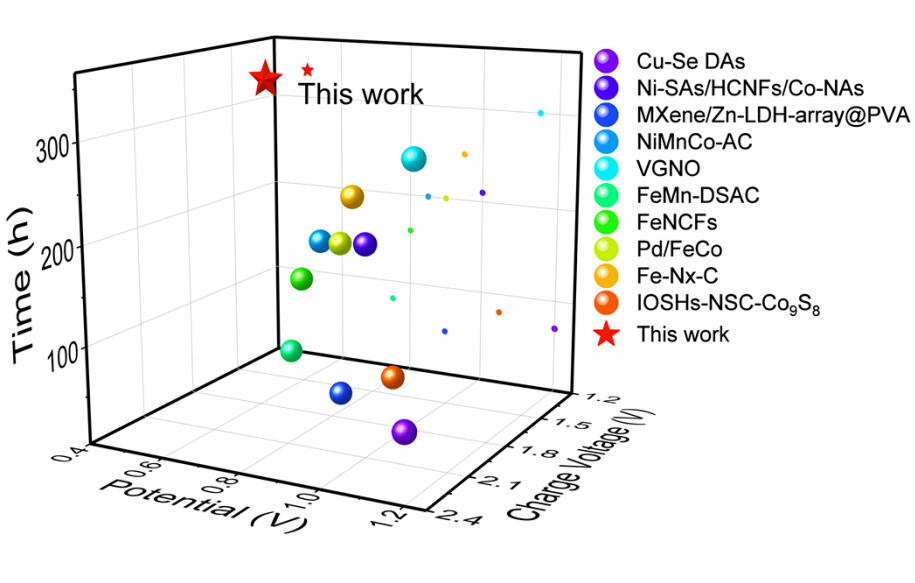

Figure S17. Comparison of the battery performance of our work with previously reported studies.[1-10]

Table S1. Performance comparison of this work with recently reported redox mediator-based ZABs in top-tier journals.[11-16]

	Voltage Gap (V)	Current Density (mA cm ^{2})	Cycle Life (h)
$Ag_{30\%}$@LCO	0.8	2	170
Co_1Fe_1-N-C+KI	0.56	10	230
$Zn(OAc)_2$+Val	1.15	10	494.5
PAAK-Gel-SC	0.82	2	108.5
KOH+PAM+KI	0.5	5	240
AEPBE	1.15	10	605
This work	0.47	10	330

Reference

1 Z. Sun, H. Zhang, L. Cao, X. Liu, D. Wu, X. Shen, X. Zhang, Z. Chen, S. Ru, X. Zhu, Z. Xia, Q. Luo, F. Xu and T. Yao, *Angew. Chem. Int. Ed.,* 2023, **62**, e202217719.

2 Y. Chen, S. Qiao, Y. Tang, Y. Du, D. Zhang, W. Wang, H. Zhang, X. Sun and C. Liu, *ACS Nano,* 2022, **16**, 15273.

3 X. Hui, P. Zhang, J. Li, D. Zhao, Z. Li, Z. Zhang, C. Wang, R. Wang and L. Yin, *Adv. Energy Mater.,* 2022, **12**, 2201393.

4 M. Jiao, Q. Zhang, C. Ye, Z. Liu, X. Zhong, J. Wang, C. Li, L. Dai, G. Zhou and H.-M. Cheng, *Proc. Natl. Acad. Sci.,* 2022, **119**, e2202202119.

5 Z. Wu, Y. Yu, G. Zhang, Y. Zhang, R. Guo, L. Li, Y. Zhao, Z. Wang, Y. Shen and G. Shao, *Adv. Sci.,* 2022, **9**, 2200614.

6 T. Cui, Y.-P. Wang, T. Ye, J. Wu, Z. Chen, J. Li, Y. Lei, D. Wang and Y. Li, *Angew. Chem. Int. Ed.,* 2022, **61**, e202115219.

7 Y. Ma, D. Chen, D. Zhang, H. Yu, Y. Zheng, W. Li, L. Wang, Q. Liu and W. Yang, *Carbon,* 2022, **187**, 196.

8 F. Pan, Z. Li, Z. Yang, Q. Ma, M. Wang, H. Wang, M. Olszta, G. Wang, Z. Feng, Y. Du and Y. Yang, *Adv. Energy Mater.,* 2021, **11**, 2002204.

9 J. Han, X. Meng, L. Lu, J. Bian, Z. Li and C. Sun, *Adv. Funct. Mater.* 2019, **29**, 1808872.

10 K. Tang, C. Yuan, Y. Xiong, H. Hu and M. Wu, *Appl. Catal. B: Environ.,* 2020, **260**, 118209.

11 J. Ran, P. Chen, X. Quan, M. Si and D. Gao, *Small*, 2024, **20**, 2402052.

12 H.-S. Fan, X. Liang, F.-X. Ma, G. Zhang, Z.-Q. Liu, L. Zhen, X. C. Zeng and C.-Y. Xu, *Small*, 2024, **20**, 2307863.

13 H. Wang, K. Wang, B. Liang, M. Wei, J. Xiong, D. Zhong and P. Pei, *Adv. Energy Mater.,* 2024, **14**, 2402123.

14 M. Fan, T. Liu, L. Lv, Z. Zheng, C. Li, G. Ma, H. Wang, H. Wan and H. Wang, *Adv. Energy Mater.*, 2026, **16**, e04476.

15 S. Zhao, J. Zhao, W. Zhang, Y. Yan, J. Ma, Q. Feng, I. T. Bello, M. Wei, T. Liu, J. Bae, M. Zhu and M. Ni, *Energy Storage Mater.*, 2024, **71**, 103630.

16 K. Ouyang, S. Chen, L. Yu, H. Qin, A. Liu, Y. Liu, Q. Wu, B. Ran, S. Wei, F. Gao, K. Zhang, J. Hu and Y. Huang, *Energy Environ. Sci.*, 2025, **18**, 4416-4430.